Flow Measurement and Instrumentation 19 (2008) 364–369

Contents lists available at ScienceDirect

Flow Measurement and Instrumentation

journal homepage: www.elsevier.com/locate/flowmeasinst

Measurement of the acoustic velocity characteristics in a standing-wave tube using out of phase PIV

Kamran Siddiqui, Majid Nabavi *

Department of Mechanical and Industrial Engineering, Concordia University, Montreal, QC, Canada, H3G 1M8

ARTICLE INFO

Article history:
Received 14 March 2008
Received in revised form
20 May 2008
Accepted 17 June 2008

Keywords:
Standing wave
Acoustic velocity field
Particle image velocimetry
Experimental analysis

ABSTRACT

The velocity fields of an acoustic standing wave in a rectangular channel are investigated. A new approach is used to measure the velocity fields using PIV. In this approach, the velocity fields are sampled at different phases in a given experimental run without synchronizing the PIV system with the excitation signal. The results show that the RMS velocities measured from this approach are in excellent agreement with the theoretical values, indicating that this new and simple approach accurately measures the RMS velocities. At the velocity antinode, the difference between the RMS measured and theoretical velocities is less than 2.4%. The results also show that this approach can be used to measure velocity fields of a standing wave in different small segments at different times and to reconstruct the entire waveform. That is, the basic statistical properties of the entire standing wave can be obtained without synchronizing PIV with the acoustic signal.

1. Introduction

When a standing acoustic wave is generated in a tube, the fluid particles oscillate under the influence of the standing wave and experience velocity and pressure variations. By exploiting the variation of these properties, the acoustic energy can be utilized to perform some useful work. For example, the acoustic energy of the standing wave in a tube has been used for refrigeration [13]. There are relatively few studies on the experimental measurements of the acoustic velocity field. Different techniques have been used to measure the acoustic particle velocities. It includes, laser Doppler anemometry (LDA) [14,17,15], hot-wire anemometry [5], condenser or piezo-electric microphone [1], pressure measurements [8] and acoustic sensor [16]. Of these techniques, LDA is a non-intrusive technique which measures the particle velocity remotely based on the intensity of the light scattered by the particles as they pass through the fringed measurement volume which is modulated at a frequency of ΔF (the frequency shift between the two laser beams). However, all these techniques provide velocity measurements at a point in space. As a result, detailed and simultaneous two-dimensional flow structure cannot be obtained from these techniques. Particle image velocimetry (PIV) provides two-dimensional velocity fields with high spatial resolution. Although PIV has been used for a variety of flow measurement applications [7], very few studies have reported the velocity measurements of the standing wave using PIV. Hann and Greated [3,4] measured particle velocities of an acoustic standing wave in a square channel at a frequency of 1616 Hz and the sound intensity of 150 dB. The camera exposure was set at 4 ms in order to capture approximately five periods of the oscillation. The particle velocities are obtained from these images by using the autocorrelation function. However, they did not present detailed velocity characteristics. Campbell et al. [2] presented a review of PIV technique with its application to the measurement of sound. Shin et al. [9] studied the velocity field of an acoustic standing wave in liquid within small tube using PIV. They conducted the study for two different liquid mediums; water and a mixture of glycol and water. The tube is square shaped with the inner dimensions of 3 mm × 3 mm. A bimorph piezo-disk is used as the acoustic driver at one end, while the other end of the tube is open. The velocity field is measured in a region 190 μm × 150 μm near the wall. The velocity fields are measured at different temporal locations with respect to the driving sinusoidal signal using a set of delay generators. Recently, Nabavi et al. [6] presented a novel approach to simultaneously measure two-dimensional acoustic and streaming velocity fields using synchronized PIV technique in any region along the resonator and at any wave phase.

To obtain velocity measurements using PIV at a specific wave phase, the laser pulses and the camera have to be synchronized with the acoustic driver. For this purpose a specialized synchronizing circuit is needed. Furthermore, to map the velocity characteristics of the entire wave using the synchronized approach, the velocity measurements have to be made at different wave phases in separate sets of experiments. At least 20 experiments at different phases have to be conducted to resolve the entire wave. In the present study we have presented a simple approach to obtain basic

* Corresponding author. Tel.: +1 514 848 2424x7102; fax: +1 514 848 3175.
E-mail address: m_nabav@encs.concordia.ca (M. Nabavi).

0955-5986/$ – see front matter © 2008 Elsevier Ltd. All rights reserved.
doi:10.1016/j.flowmeasinst.2008.06.001

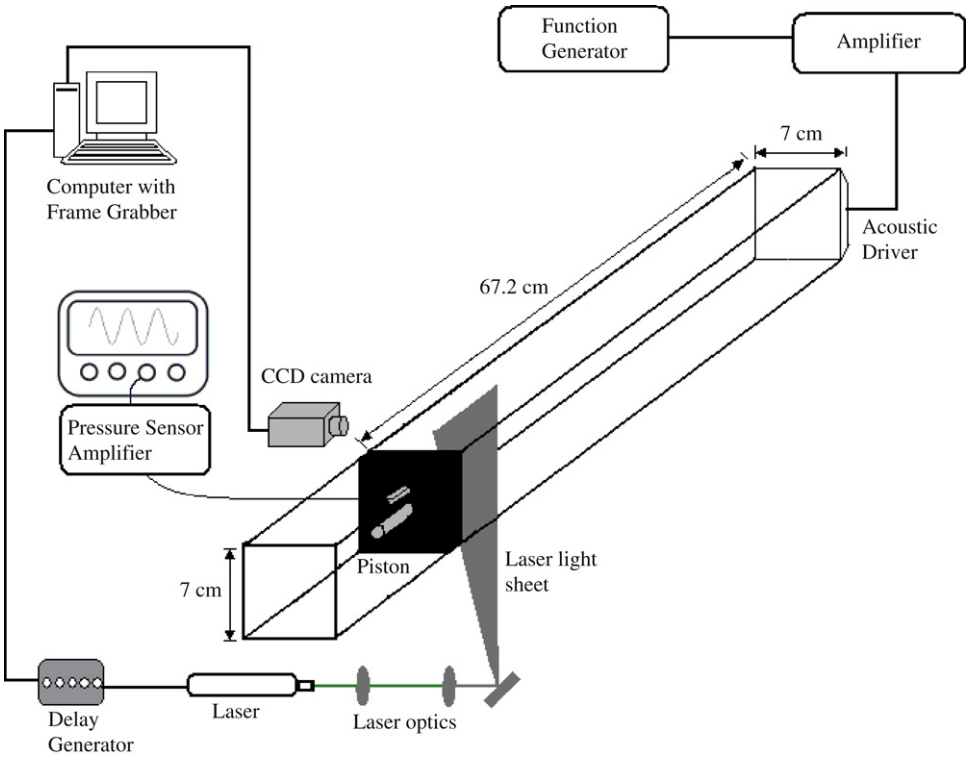

Fig. 1. Schematic of the experimental setup and instrumentation.

statistical properties of the entire standing wave without synchronizing PIV with the acoustic signal. In addition to the simplicity of the experimental setup and instrumentation, another advantage of the proposed approach is that the sample size to compute the RMS velocity at any spatial location is significantly larger than that for the synchronized approach.

2. Experimental setup

Experiments are conducted in a Plexiglas channel of square cross-section. The inner cross-section of the channel is 7×7 cm. An 8 Ω electro-dynamic type loudspeaker with the maximum power of 50 W is used as the acoustic driver. A function generator model Agilent 33120A is used to generate the sinusoidal wave. The signal from the function generator is amplified by an amplifier (MPA-25, Realistic). The loudspeaker is driven by this amplified signal. A movable piston is attached to the other end of the channel, which allowed to change the length of the channel depending on the frequency of the acoustic driver (see Fig. 1). In the present study, the length of the channel is set equal to twice the wavelength at a given frequency to allow the formation of two complete standing waves inside the channel. Air at the atmospheric pressure is used as the working fluid. The acoustic pressure is measured by a condenser microphone cartridge Model 377A10 PCB Piezotronics. The microphone consists of a microphone cartridge and a microphone preamplifier. A preamplifier Model 426B03 is used in order to measure the sound pressure level. The cartridge screws directly onto the preamplifier housing. The frequency response is almost flat between 5 Hz and 100 kHz. During the experiments, the microphone is placed inside a hole in the adjustable piston and flashed with the piston inner surface. Thus, the microphone and piston are always at the same position i.e. at the pressure antinode, and the microphone measures the maximum pressure fluctuation (see Fig. 1).

The thickness of the channel walls is 6 mm. To confirm that the rigid wall assumption holds for this channel, the wall vibration is measured using a Brüel & Kjær laser vibrometer. The laser vibrometer consists of a Helium–Neon laser velocity transducer type 8323, a power supply type 2815 and a signal analyzer unit type 2035. The maximum wall displacement is found to be approximately one micron which is approximately 200 times less than the maximum displacement of the acoustic driver. Thus, it is concluded that the channel walls are rigid under the given experimental conditions.

The two-dimensional velocity fields inside the channel are measured using particle image velocimetry (PIV). The measurements are made in a plane parallel to the channel length at the mid-channel location (i.e. 3.5 cm from both vertical walls of the channel) as shown in Fig. 1. A Continuum Minilite 25 mJ Nd:YAG laser is used as a light source for the PIV measurements. A CCD camera (JAI CV-M2) with the resolution of 1600×1200 pixels is used to image the flow. The camera is connected to a PC equipped with a frame grabber (DVR Express, IO Industries, London, ON, Canada) that acquired 8-bit images at a rate of 30 Hz. A four-channel digital delay generator (555-4C, Berkeley Nucleonics Corporation, San Rafael CA) is used to control the timing of the laser light pulses. Olive oil mist with the mean diameter of 0.5 μm is used as the tracer particles. An aerosol generator (Lavision Inc., Ypsilanti MI) is used to generate the oil mist.

An important issue related to the tracer particles is their response time. That is, how quickly the particles respond to any change in the flow behavior. In the present study, the density of the tracer particles is much higher than that of the air; therefore, it is important to find the response time of particles. Furthermore, as the particles oscillate under the action of the standing wave, this issue becomes even more critical. The characteristic response time of the seed particles is computed by,

$$T_P = \frac{u_T}{g} \tag{1}$$

where, T_P is the particle response time, u_T is the particle terminal velocity and g is the acceleration due to gravity [12]. The terminal

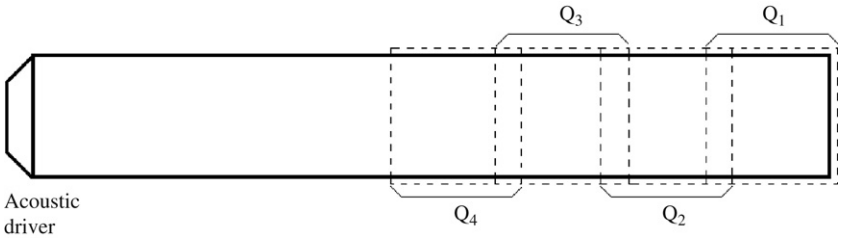

Fig. 2. Fields of view of the CCD camera for PIV measurements in different sections. The size of the field of view is same for all sections (i.e. 11.2 cm in horizontal and 8.4 cm in vertical). However, the overlap between any two sections is not constant.

velocity is computed by,

$$u_T = \frac{(\gamma - 1)D^2 g}{18\nu} \tag{2}$$

where D is the diameter of the tracer particles, ν is the kinematic viscosity of the fluid and γ is the ratio of the density of particle to the density of fluid [11]. Using the above equations, it is found that for $D = 0.5\ \mu$m, $u_T = 7\ \mu\text{m s}^{-1}$ and $T_p = 0.7\ \mu$s. For the driver frequency of 1040 Hz (time period $= 961\ \mu$s), the particle response is approximately 1400 times faster than the time period of the acoustic wave. Thus, we conclude that the tracer particles accurately follow the flow.

Shin et al. [9] estimated the errors in the PIV acoustic velocity measurement based on the error due to slip and error due to Brownian motion. We followed the same approach to compute the error in the present velocity measurements. The error due to slip is based on the difference between the fluid and particle velocities. This is identical to the particle response time estimated above. Using this analysis we found that for the given conditions with the particle diameter of 0.5 μm, the maximum particle slip or the maximum difference between the fluid and particle velocities is 0.011 m/s. For the maximum velocity of approximately 2.4 m/s, the maximum error due to slip is 0.46%. Shin et al. [9] found that the error due to the Brownian motion is insignificant in their experiments. In the present study, we found that the error due to Brownian motion is equal to 0.074% which is insignificant and consistent with the observation of [9].

The wavelength of the acoustic standing wave corresponds to the driver frequency of 1040 Hz is 33.08 cm. As mentioned earlier, the length of the channel is adjusted to allow the formation of two full standing waves in the channel. If the field of view of the CCD camera is set in a way to measure the velocity field of the entire wave, the resolution of the velocity vectors decreases significantly. In addition, the particle displacement between the two images of an image pair reduces which increases the uncertainty in the PIV velocity measurements. The field of view of the camera is set in a way to measure the velocity field within the entire height of the channel. That is, the field of view of the camera is set equal to 11.2 cm in horizontal and 8.4 cm in vertical. The horizontal dimension of the camera field of view is less than the wavelength of the standing wave. In order to map the flow field of the entire wave, the measurements are made at four different horizontal locations that cover all regions of the wave. The first set of measurements is made in the region adjacent to the wall (piston end). In the subsequent sets, the region of interest is shifted towards the driver end with an overlap between the adjacent regions of interest. Hereinafter these sets are referred to as Q_1, Q_2, Q_3 and Q_4 (see Fig. 2).

As mentioned earlier, in the present study, we adapted a different and simple approach from the experimental view point to measure the velocity fields. In this approach, the acoustic driver is not synchronized with the laser pulses. That is, the data acquisition is started at a random phase for every experimental run (i.e. at each section). Furthermore, the PIV technique measures velocity fields at 15 Hz which is not the integer multiple of the given standing-wave frequency (i.e. 1040 Hz). Therefore, during each experimental run, the velocity fields are sampled at different phases of the standing wave. For each set of measurements, 1800 velocity fields are obtained (i.e. the total sampling time of two minutes).

The selection of the proper separation time between the two images of an image pair is important. Due to the oscillation of the particles, the time separation between the two images of an image pair must be much smaller than the quarter of the time period. Otherwise, the particle displacement computed by cross-correlating the PIV images will be smaller than the actual displacement of the particles. This will result in the underestimated velocities. On the other hand, for very short separation time, the particle displacement will be too small that will significantly increase the uncertainty in the velocity measurements. For the given frequency, the time separation is set equal to 80 μs which is a factor of three smaller than the quarter wave period.

The height of the camera field of view is greater than the height of the channel. Before computing the velocity vectors, the images are preprocessed to remove the regions outside the channel. That is, all the regions above the inner surface of the upper wall and below the inner surface of the lower wall are chopped off. Thus after preprocessing, the PIV images consist of only the inner region of the channel. The PIV technique computes velocity vectors by cross-correlating the interrogation region in the first image with the corresponding search region in the second image of an image pair. In the present study, the size of the interrogation region is set equal to 32 ×32 pixels and the size of the search region is set equal to 64 ×64 pixels. A 50% window overlap is used in order to increase the nominal resolution of the velocity field to 16 ×16 pixels. This resulted in the spatial resolution of 1.1 ×1.1 mm of the velocity field. This provides very high spatial resolution for the given wave that is, the velocity field is resolved at approximately 300 locations along the entire wave. A three-point Gaussian sub-pixel fit scheme is used to obtain the correlation peak with sub-pixel accuracy. A scheme is used to identify the spurious velocity vectors and then correct them using a local median test [10]. Less than 1% of the velocity vectors are spurious.

3. Results

An instantaneous two-dimensional velocity field in the region adjacent to the piston (i.e. section Q_1) is shown in Fig. 3(a). The plot shows that the velocity magnitude decreases when approaching the piston and becomes almost zero immediately adjacent to the piston. This is an expected behavior as the pressure fluctuations are maximum at the piston (i.e. pressure antinode). Moving from right to left in the plot, the velocity increases up to a certain distance and then starts decreasing. The maximum velocity occurs at the location where the pressure fluctuations are minimum. In the present figure, the maximum velocity is located at 8.25 cm from the piston end. The depth-averaged horizontal velocity of the velocity field in Fig. 3(a) is shown in Fig. 3(b). The horizontal

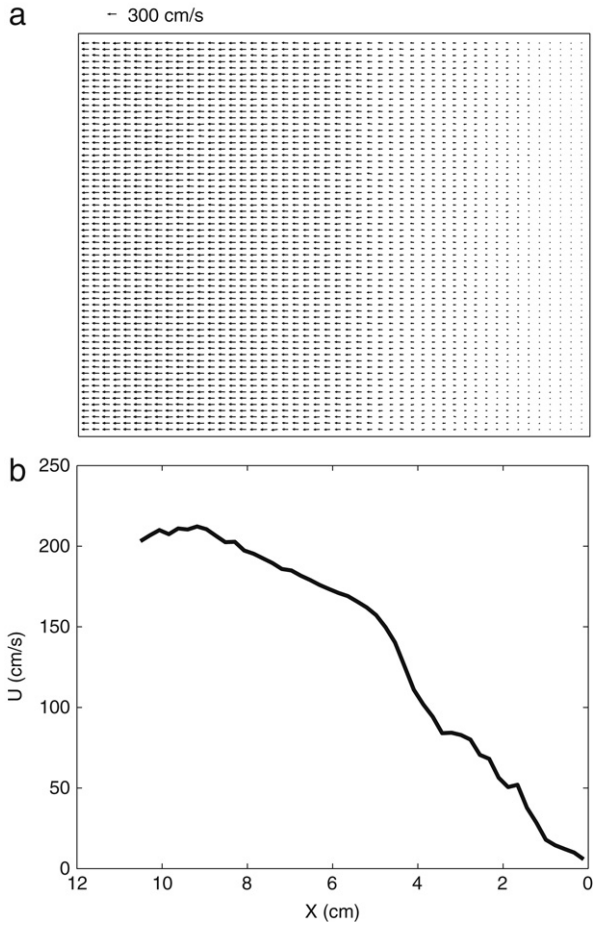

Fig. 3. (a) An instantaneous velocity field in section Q_1. (b) The depth-averaged horizontal velocity of the plot shown in (a). X is the distance measured from the piston wall (closed end).

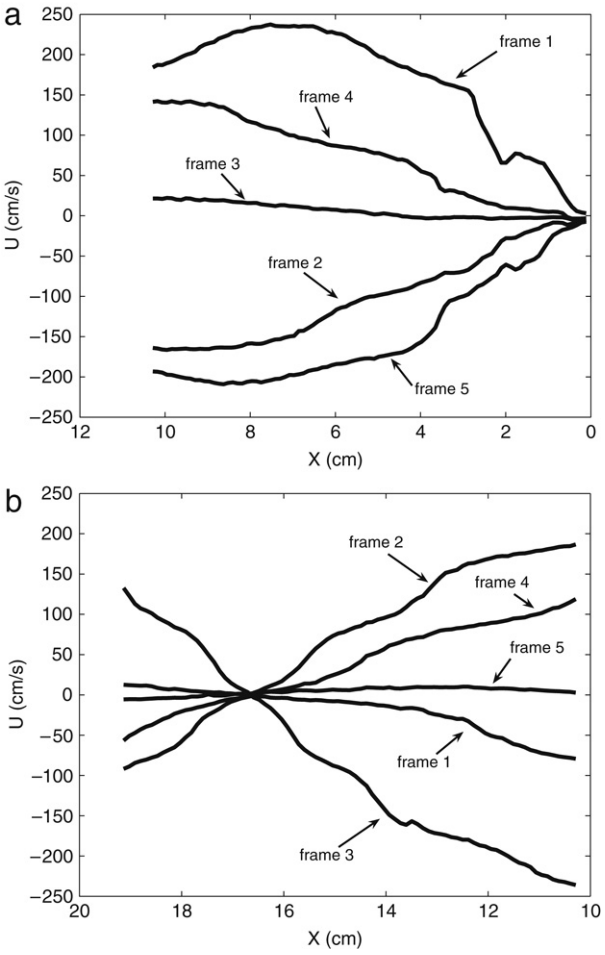

Fig. 4. The depth-averaged horizontal velocity in consecutive velocity fields in, (a) section Q_1, (b) section Q_2. The time difference between each frame is 1/15 s. The frames in shown in (a) and (b) are taken at different times. X is the distance measured from the piston wall (closed end).

velocity shows the behavior of a typical standing wave. Since the PIV measurements provide velocity field in a two-dimensional plane, the cross-channel variations in the horizontal velocity are also analyzed. These variations are found to be in the range 3–6 cm/s which are insignificant compared to the horizontal velocity magnitude.

As mentioned in the previous section, the acoustic driver is not synchronized with the laser pulses and the PIV sampling frequency is not the multiple of the standing-wave frequency. Therefore, the present dataset comprised velocity fields measured at different phases of the standing wave. The depth-averaged horizontal velocity profiles in some consecutive velocity fields in sections Q_1 and Q_2 are shown in Fig. 4. Note that the same frame numbers in Q_1 and Q_2 do not represent the same time as the velocity fields in each section is computed in separate sets of experiments at different times. The plots show that the successive frames captured the velocity fields at different phases of the standing wave. At each section, 1800 velocity fields are measured. This sample size is large enough to represent the velocity fields at different phases of the standing wave and thus provides good statistical information about the standing-wave-velocity characteristics.

The root-mean-square (RMS) horizontal velocity of the complete standing wave is shown in Fig. 5. The velocity profile of the complete wave is obtained by combining the RMS velocity profiles computed in sections Q_1, Q_2, Q_3 and Q_4. The overlapping regions between the two adjacent sections are marked with the thin straight lines. The excellent matching of the data in the overlapping regions confirms that the number of velocity fields in each section is large enough to provide reliable statistical properties of the given standing wave. It should also be noted that the data acquisition in each section is started at a random phase. The results also indicate that the statistical characteristics of the full standing wave can be obtained by combining the statistical characteristics that are computed in different sections of the wave at different times. The plot shows that the RMS velocities approach zero at the pressure antinodes which are located at $\lambda = 0, \frac{1}{2}$ and 1, where λ is the wavelength of the standing wave. Similarly, the maximum velocities are observed at velocity antinodes which are located at $\lambda = \frac{1}{4}$ and $\frac{3}{4}$.

To confirm that the velocities obtained from the given approach (i.e. by sampling at different wave phases) are accurate, the velocity characteristics from the experimental data are compared with that obtained from the exact analytical solution. For a tube filled with a fluid, the particle velocity under the action of acoustic wave is given by,

$$u(x,t) = -(1/\rho)\int(\partial p/\partial x)\mathrm{d}t \tag{3}$$

where, ρ is the density of the fluid and $p(x,t)$ is the pressure. For the given case, the boundary conditions are $p(0,t) = P_0\cos\omega t$, and $u_x(L,t) = 0$, where, P_0 is the pressure amplitude at the acoustic driver, L is the length of the channel, ω is the radian frequency and u_x is the velocity derivative with respect to x. For the given boundary conditions, the pressure is given by,

$$p(x,t) = P_0\frac{\cos k(L-x)}{\cos kL}\cos\omega t \tag{4}$$

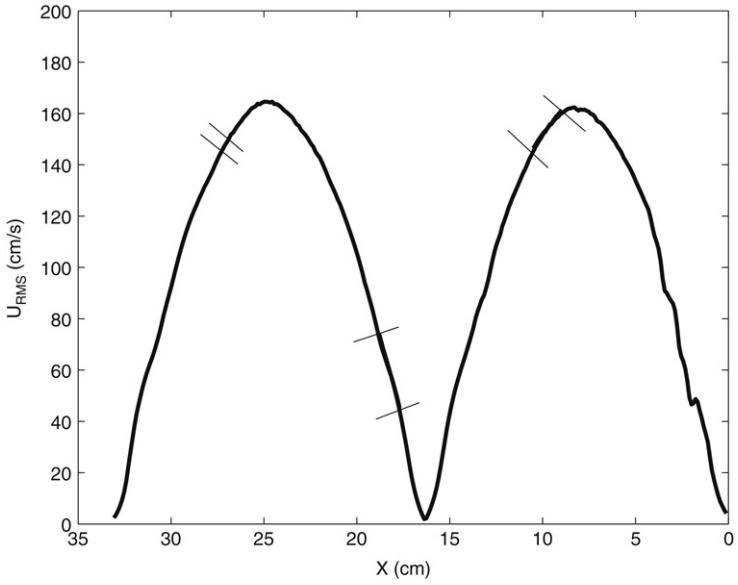

Fig. 5. The root-mean-square (RMS) horizontal velocity of the complete wave obtained by combining the RMS horizontal velocities in each section. The thin lines represent the overlap region between two adjacent sections. X is the distance measured from the piston wall (closed end).

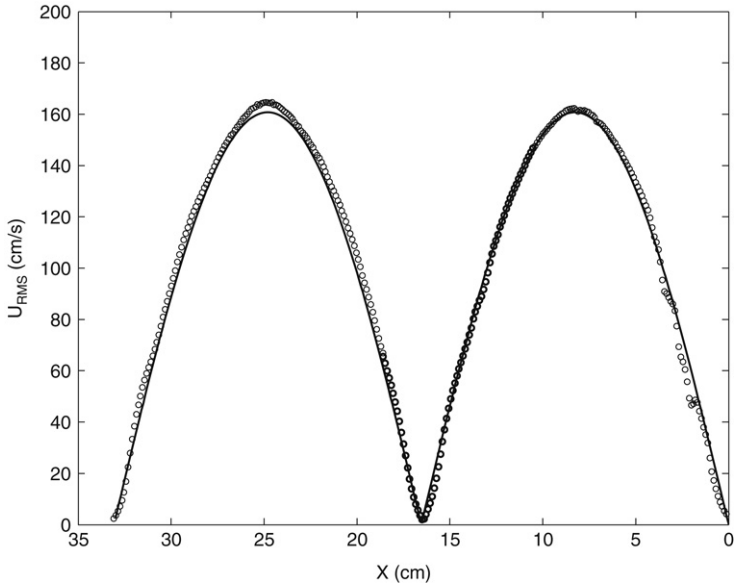

Fig. 6. The comparison between the theoretical and experimental RMS horizontal velocities at a frequency of 1040 Hz. Solid line, theoretical; ◯, experimental. X is the distance measured from the piston wall (closed end).

where, $k = \omega/c$ and c is the speed of sound. Substituting $p(x, t)$ from Eq. (4) into Eq. (3), the particle velocity is given by,

$$u(x, t) = u_0 \frac{\sin k(L - x)}{\cos kL} \sin \omega t \tag{5}$$

where, $u_0 = P_0/\rho c$. The uncertainty in the estimation of u_0 is due to the uncertainties in the pressure measurement, position of the microphone relative to the pressure node and the change in air density due to seed particles. The total uncertainty in u_0 is estimated to be less than 5%.

All experiments are conducted in air at 25 °C ($c = 344$ m/s, $\rho = 1.2$ kg/m^3). The value of P_0 for this case is 938 Pa. The RMS velocities from the experiments and analytical solution are plotted in Fig. 6. The results show a good agreement between the experimental and theoretical results, which confirms that the given approach accurately measures the RMS velocities of the standing wave. At the velocity antinode, the RMS velocities are up to 2.4% higher than the theoretical values.

To further confirm that the proposed technique is capable of measuring the acoustic velocity field accurately, we have conducted another set of experiments in another channel. This channel is 105 cm long with the cross-section of 4 ×4 cm. The experiments are conducted at a frequency of 976 Hz. The corresponding wavelength is 35.2 cm. This results in the formation of three full standing waves inside the channel. The field of view of the camera is set equal to 10.3 cm in horizontal and 8 cm in vertical to map the flow field in the quarter-wavelength section of the channel. The separation time between two PIV images of the image pair is set equal to 80 μs. The value of P_0 for this case is 640 Pa. The RMS velocities for this case are plotted in Fig. 7. The RMS velocities obtained from the analytical solution for the given conditions are also plotted in the figure for comparison. At the velocity antinode, the experimentally obtained RMS velocities are 2.2% lower than the theoretical values.

Good agreement between the experimental and analytical results for different frequencies, excitation amplitudes and channel

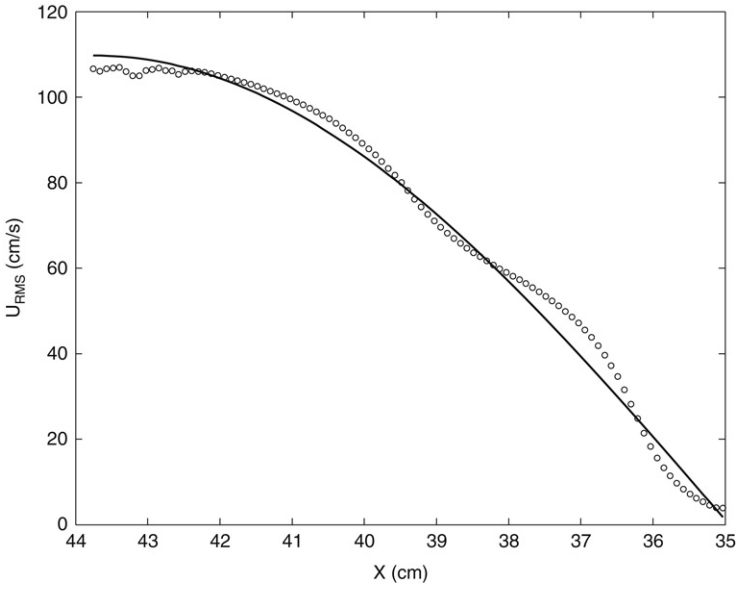

Fig. 7. The comparison between the theoretical and experimental RMS horizontal velocities at a frequency of 976 Hz in quarter-wavelength section of the second channel. Solid line, theoretical; ◯, experimental. *X* is the distance measured from the piston wall (closed end).

dimensions (Figs. 6 and 7) confirms that the given approach (i.e. out of phase PIV) correctly measures the RMS acoustic velocities.

4. Conclusions

The velocity fields of an acoustic standing wave in a tube are investigated. A new approach is used to measure the velocity fields. In this approach, the PIV system is not synchronized with the acoustic wave signal and therefore, the velocity fields are sampled at different phases in a given experimental run. The experimental setup and instrumentation for the present approach is simple and the RMS velocity at any spatial location is obtained from a larger sample size compared to the synchronized approach, which improves its accuracy. The limitation of this approach is that the velocity field at a particular phase cannot be resolved. The results show that the RMS velocities measured using this approach are in excellent agreement with the theoretical values, indicating that this new and simple approach accurately measures the RMS velocities of the acoustic standing wave. At the velocity antinode, the difference between the RMS measured and theoretical velocities is less than 2.4%. The results also show that this approach can be used to measure velocity fields of a standing wave in different small segments at different times and to reconstruct the entire waveform. This enables measuring the velocity fields of longer standing waves with high spatial resolution.

References

[1] Bies AD, Hansen CH. Engineering noise control, theory and practice. London: E&FN Spon Press; 1996.
[2] Campbell M, Cosgrove JA, Greated CA, Rockliff JD. Review of LDA and PIV applied to the measurement of sound and acoustic streaming. Optics Laser Technol 2000;32:629–39.
[3] Hann DB, Greated CA. Particle image velocimetry for the measurement of mean and acoustic particle velocities. Meas Sci Technol 1997;8:656–60.
[4] Hann DB, Greated CA. The measurement of flow velocity and acoustic particle velocity using particle image velocimetry. Meas Sci Technol 1997;8:1517–22.
[5] Huelsz G, Lopez-Alquicira F. Hot-wire anemometry in acoustic waves. Experiments Fluids 2001;30:283–5.
[6] Nabavi M, Siddiqui MHK, Dargahi J. Simultaneous measurements of streaming and acoustic velocity fields using synchronized PIV. Meas Sci Technol 2007; 18:1811–7.
[7] Ozalp C, Pinarbasi A, Fakilar MS, Sahin B. PIV measurements of flow through a sudden contraction. Flow Measurement Instrumentation 2007;18:121–8.
[8] Pierce AD. Acoustics, an introduction to its physical principles and applications. Acoust Soc Am 1994.
[9] Shin Y, Jaewon C, Domoto GA, Grigoropoulos CP. Compressible flow of liquid in a standing wave tube. J Fluid Mech 2005;536:321–45.
[10] Siddiqui MHK, Loewen MR, Richardson C, Asher WE, Jessup AT. Simultaneous particle image velocimetry and infrared imagery of microscale breaking waves. Phys Fluids 2001;13:1891–903.
[11] Siegel DA, Plueddemann AJ. The motion of a solid sphere in an oscillating flow: An evaluation of remotely sensed doppler velocity estimates in the sea. J Atmos Oceanic Technol 1991;8:296–304.
[12] Snyder WH, Lumley JL. Some measurements of particle velocity autocorrelation functions in a turbulent flow. J Fluid Mech 1971;48:41–71.
[13] Swift GW. Thermoacoustics Acoust Soc Ame 2002.
[14] Taylor KJ. Absolute measurement of acoustic particle velocity. J Acoust Soc Am 1976;59:691–4.
[15] Thompson MW, Atchley AA. Simultaneous measurement of acoustic and streaming velocities in a standing wave using laser Doppler anemometry. J Acoust Soc Am 2005;117:1828–38.
[16] van der Eerden FJM, de Bree H-E, Tijdeman H. Experiments with a new acoustic particle velocity sensor in an impedance tube. Sensors Actuators A 1998;69: 126–33.
[17] Vignola JF, Berthelot YH, Jarzynski J. Laser detection of sound. J Acoust Soc Am 1990;90:1275–86.